



**HAL**  
open science

## **IRAP+ endosomes restrict TLR9 activation and signaling**

Joël Babdor, Delphyne Descamps, Adiko Assi Aimé Cézaire, Mira Tohmé, Sophia Maschalidi, Irimi Evnouchidou, Luiz Ricardo Vasconcellos, Mariacristina de Luca, Francois-Xavier Mauvais, Meriem Garfa-Traore, et al.

### ► To cite this version:

Joël Babdor, Delphyne Descamps, Adiko Assi Aimé Cézaire, Mira Tohmé, Sophia Maschalidi, et al.. IRAP+ endosomes restrict TLR9 activation and signaling. *Nature Immunology*, 2017, 18 (5), pp.509-518. 10.1038/ni.3711 . inserm-01674784

**HAL Id: inserm-01674784**

**<https://inserm.hal.science/inserm-01674784>**

Submitted on 3 Jan 2018

**HAL** is a multi-disciplinary open access archive for the deposit and dissemination of scientific research documents, whether they are published or not. The documents may come from teaching and research institutions in France or abroad, or from public or private research centers.

L'archive ouverte pluridisciplinaire **HAL**, est destinée au dépôt et à la diffusion de documents scientifiques de niveau recherche, publiés ou non, émanant des établissements d'enseignement et de recherche français ou étrangers, des laboratoires publics ou privés.

## IRAP+ endosomes restrict Toll2like receptor 9 activation and signaling

Joel Babbord<sup>1,2,3&</sup>, Delphine Descamps<sup>1,2,3,4&</sup>, Adiko Assi Aimé Cézaire<sup>5,6</sup>, Mira Tohmé<sup>1,2,3,7</sup>,  
Sophia Maschalidi<sup>1,2,3,8</sup>, Irini Evnouchidou<sup>5,6</sup>, Luiz Ricardo Vasconcellos<sup>1,2,3,9</sup>, Mariacristina  
De Luca<sup>5,6</sup>, Francois-Xavier Mauvais<sup>1,2,3</sup>, Meriem Garfa-Traore<sup>1,2,3</sup>, Melanie M. Brinkmann<sup>10</sup>,  
Michel Chignard<sup>11,12</sup>, Bénédicte Manoury<sup>1,2,3,#,\*</sup>, Loredana Saveanu<sup>5,6,#,\*</sup>

1. Institut National de la Santé et de la Recherche Médicale, Unité 1151, Paris, 75015, France
2. Centre National de la Recherche Scientifique, Unité 8253, Paris, 75015, France
3. Université Paris Descartes, Sorbonne Paris Cité, Faculté de médecine Paris Descartes, 75015 Paris, France
4. VIM, INRA, Université Paris-Saclay, 78350, Jouy-en-Josas, France.
5. Institut National de la Santé et de la Recherche Médicale, Unité UMR 1149, Centre de Recherche sur l'Inflammation, Paris, France
6. Université Paris Diderot, Faculté de Médecine Xavier Bichat, Paris, France
7. Division of Immunology, Boston Children's Hospital, Department of Pediatrics, Harvard Medical School, Boston, Massachusetts, USA
8. Laboratory of Normal and Pathological Homeostasis of the Immune System, INSERM UMR1163, Paris, France
9. Laboratório de Imunoreceptores e Sinalização, Instituto de Biofísica Carlos Chagas Filho, Universidade Federal do Rio de Janeiro, Rio de Janeiro RJ 21.941-902, Brazil;
10. Helmholtz Centre for Infection Research, 38124 Braunschweig, Germany
11. Institut National de la Santé et de la Recherche Médicale, UMR S 938, CDR Saint-Antoine, Paris, France
12. Sorbonne Université, UPMC Univ Paris 06, UMR S 938, CDR Saint-Antoine, Paris, France

& Co-first authors

# Co-senior authors

\* Correspondence to: Loredana Saveanu, INSERM, Unité 1149, Faculté de Médecine Bichat, 16 rue Henri Huchard, 75018, Paris cedex 18, France

Bénédicte Manoury, INSERM, Unité 1151, Hôpital Necker-Enfants malades, 149 rue de Sèvres, 75743 Paris cedex 15, France

Emails: [loredana.saveanu@inserm.fr](mailto:loredana.saveanu@inserm.fr), [benedicte.manoury@inserm.fr](mailto:benedicte.manoury@inserm.fr)

## **Abstract**

Retention of intracellular Toll-Like Receptors (TLRs) in the endoplasmic reticulum prevents their activation under basal conditions. TLR9 is activated by sensing ligands in specific endosomal/lysosomal compartments. Here, we describe the identification of insulin responsive aminopeptidase (IRAP) endosomes as major cellular compartments for the early steps of TLR9 activation in dendritic cells (DCs). Both TLR9 and its ligand CpG were found as cargo in IRAP endosomes. In the absence of IRAP, CpG and TLR9 trafficking to lysosomes and TLR9 signaling were enhanced in DCs and in mice following bacterial infection. IRAP stabilized CpG-containing endosomes by interacting with the actin nucleation factor FHOD4, slowing down TLR9 trafficking towards lysosomes. Thus, endosome retention of TLR9 via IRAP interaction with the actin cytoskeleton is a mechanism that prevents TLR9 hyper-activation in DCs.

Innate and adaptive immune responses depend on the ability of toll-like receptors (TLRs) to discriminate between different classes of microbial products and initiate specific signaling cascades. While microbial products with no equivalent in mammalian cells, such as the components of the bacterial wall, are recognized by surface TLRs (1, 2, 4, 5 and 6), pathogen derived nucleic acids are sensed by intracellular TLRs (3, 7, 8 and 9). Recognition of nucleic acids by intracellular TLRs has the potential to trigger autoimmune diseases through interaction with self nucleic acids<sup>1</sup>. To avoid inappropriate activation of endosomal TLRs, their trafficking is tightly controlled. Thus, in basal conditions the receptors are located in the endoplasmic reticulum (ER) and translocate to endocytic vesicles only after cell stimulation by TLR ligands. Although all intracellular TLRs reside in the ER<sup>2,3</sup>, the trafficking pathways that move the receptors into the endocytic pathway show considerable variation among intracellular TLRs<sup>4-6</sup>. For example, TLR7 traffics from Golgi stacks directly to endosomes using the clathrin adaptor AP4, whereas the TLR9 is directed to the cell surface and reaches the endosomes via AP2-mediated clathrin-dependent endocytosis<sup>6</sup>.

In addition to the transfer into the endocytic pathway, a second step that controls the activation of endosomal TLRs is their partial proteolysis by an array of different proteases, specific for each TLR<sup>5,7-12</sup>.

Although less often mentioned, the intracellular trafficking of its ligand also controls the activation of TLR9. TLR9 ligands (CpG) are internalized via clathrin-mediated endocytosis in early endosomes and translocate to late LAMP<sup>+</sup> compartments<sup>2</sup>. TLR9 activation depends on CpG localization, since the abrogation of CpG translocation to LAMP<sup>+</sup> compartments by specific inhibitors decreased TLR9 signaling<sup>13,14</sup>. Thus, the intracellular trafficking of both, the ligand and the receptor are essential for the control of TLR9 activation.

The complexity of TLR9 and CpG trafficking is rendered possible by the diversity and plasticity of the endocytic system. This system includes early endosomes that fuse to generate the sorting endosomes. From there, cargos are directed to different organelles, such as Rab4<sup>+</sup> fast recycling endosomes, Rab11<sup>+</sup> slow recycling endosomes, the *trans*-Golgi network (TGN) or lysosomes. Next to these universal routes of endosome trafficking, specialized cells, such as dendritic cells (DCs), display particular, albeit poorly characterized endosomal populations that affect TLR function, such as the VAMP3<sup>+</sup> vesicles, which are involved in TLR9 trafficking<sup>15</sup>.

A particular and abundant endocytic population present in DCs, not yet investigated in the context of TLR signaling, is the slow recycling endosomes. They are characterized by the

presence of the aminopeptidase IRAP (Insulin Responsive AminoPeptidase), a type II transmembrane protein composed of a catalytic site localized in the endosomal lumen and a cytosolic domain of 110 amino acids. In DCs, IRAP<sup>+</sup> endosomes are rapidly recruited to DC phagosomes, where the enzymatic activity of IRAP is involved in antigen processing during MHC-I cross-presentation<sup>16,17</sup>.

The regulated trafficking of IRAP depends on the cytosolic domain of the enzyme, which has been shown to interact with several proteins involved in vesicle formation or in cytoskeleton remodeling, such as the golgin p115<sup>18</sup>, vimentin<sup>19</sup> and FHOS (formin homologue overexpressed in the spleen, also called FHOD1)<sup>20</sup>. Whether these proteins and their interaction with the cytosolic domain of IRAP play a role in the trafficking of IRAP<sup>+</sup> endosomes is not known.

We wondered if IRAP plays a role in endosomal TLR trafficking and activation. We report here that the early steps in TLR9 trafficking and CpG endocytosis require IRAP. The absence of IRAP affected both CpG and TLR9 trafficking, leading to a dramatic increase in TLR9 signaling *in vitro* and *in vivo* following TLR9 stimulation. Thus, by anchoring TLR9 endosomes to the actin cytoskeleton, IRAP limited TLR9 activation. These findings provide a mechanistic explanation for the link between IRAP mutations and autoimmune disorders implicating TLR9<sup>21</sup> and identify new factors and cellular pathways involved in TLR9 activation.

## RESULTS

### IRAP deletion increases TLR9 response

To address the role of IRAP in TLRs signaling, wild-type and IRAP-deficient bone marrow derived dendritic cells (BMDCs) were stimulated with specific TLR ligands: polyIC for TLR3, Imiquimod for TLR7, CpG-B for TLR9 and LPS for TLR4, and the production of the pro-inflammatory cytokines IL-6, IL-12p40, TNF was measured. Although IRAP deletion did not affect TLR3- and TLR4-dependent pro-inflammatory cytokine production, it enhanced pro-inflammatory cytokine production driven by TLR9 (**Fig. 1a**) and TLR7 activation (**Supplementary Fig. 1a**). These results suggest that IRAP affects the NF-κB pathway downstream of TLR9 and probably also TLR7.

Since type I interferon (IFN) production depends on TLR9 signaling through IRF7, we wondered whether IRAP deletion affected this cytokine. We measured IFN-β production by wild-type and IRAP-deficient BMDCs stimulated with TLR3, 4 and 9 ligands (**Fig. 1b**).

IRAP deletion significantly increased only TLR9-driven IFN- $\beta$  production but not IFN- $\beta$  production by TLR3 and TLR4. Thus, IRAP disturbed the amplitude of both pro-inflammatory cytokine and type I IFN production in a TLR9-dependent manner in BMDCs.

To address whether the hypersensitivity of IRAP-deficient cells to TLR9 ligands was restricted to BMDCs, we purified conventional DCs (cDCs) and plasmacytoid DCs (pDCs) from the spleen and stimulated them with a TLR9 agonist. When incubated with CpG, IRAP-deficient spleen cDCs (**Fig. 1c**) and pDCs (**Fig. 1d**) produced significantly higher amounts of pro-inflammatory cytokines and INF- $\alpha$  than their wild-type counterparts. These results demonstrated that IRAP controls TLR9 activation in all tested DC subsets.

At least two mechanisms could account for the increased TLR9 response in IRAP-deficient DCs. IRAP<sup>+</sup> endosomes could store pro-inflammatory cytokines and control their secretion or directly influence TLR9 or CpG trafficking. We analyzed the intracellular localization of pro-inflammatory cytokines in wild-type and IRAP-deficient cells. Neither IL-12, nor IL-6 colocalized with IRAP, but they were found in Golgi stacks, as previously reported (**Supplementary Fig. 1b-c**)<sup>22</sup>. Thus, IRAP<sup>+</sup> endosomes are unlikely to be implicated in trafficking or secretion of IL-6 or IL-12p40 and could be involved in a step upstream of their synthesis. In support of this hypothesis, we found that DCs lacking IRAP expressed significantly higher levels of pro-inflammatory cytokine mRNAs than wild-type DCs upon CpG but not LPS stimulation (**Fig. 1e-f**).

The increase in cytokines mRNA in IRAP deficient cells following TLR9 stimulation should be correlated with enhanced TLR9 signaling. To specifically investigate TLR9 signaling, we tested the association of the MyD88 adaptor with the transcription factors NF- $\kappa$ B and IRF7. A proximity ligation assay which detects protein complexes *in situ*<sup>23</sup>, demonstrated a significantly increased association of MyD88 with NF- $\kappa$ B (**Fig. 2a**) and of MyD88 with IRF7 (**Fig. 2b**) in IRAP-deficient cells, as compared with wild-type cells.

As a consequence of TLR activation, the mitogen-activated protein kinase ERK is rapidly phosphorylated. Indeed, ERK phosphorylation was increased in IRAP deficient cells after CpG stimulation, as detected by immunoblot (**Fig. 2c**). In addition, the last step of NF- $\kappa$ B activation, the phosphorylation of I $\kappa$ B- $\alpha$ , was also significantly increased in IRAP-deficient cells after CpG but not LPS treatment (**Fig. 2d**). Altogether, these results indicate an enhanced TLR9 signaling in the absence of IRAP.

### **IRAP-deficient mice display a TLR9 inflammatory phenotype**

Our *in vitro* data demonstrated the regulation of TLR9 signaling by IRAP. We next addressed whether IRAP-deficient mice (*Lnpep*<sup>-/-</sup>) display increased TLR9 activation. To test this, we measured IL-6 in the serum of wild-type and IRAP-deficient mice 2 h after intravenous injection of PBS, CpG-B or LPS. Although wild-type and IRAP-deficient animals responded identically to PBS and LPS injection, TLR9 stimulation led to higher IL-6 in the serum of mice lacking IRAP than in wild-type animals (**Fig. 3a**).

We wondered if the exacerbated proinflammatory TLR9 signaling might affect the innate immune response during a bacterial infection. *Pseudomonas aeruginosa* is a Gram-negative bacterium that activates several TLRs including TLR9 on alveolar macrophages (AM) and epithelial cells<sup>24</sup>. TLR9-deficient mice were shown to be resistant to *P. aeruginosa* infection, suggesting that TLR9 signaling can have deleterious effects in this model<sup>25</sup>. In order to test whether TLR9-dependent hyperactivation observed in IRAP-deficient mice could affect survival upon bacterial pulmonary infection, we intranasally inoculated IRAP-deficient and wild-type mice with 10<sup>6</sup> CFU of *P. aeruginosa* and monitored them for survival. At least 36% of wild-type mice survived during the two weeks of observation, while all IRAP-deficient mice died within 72 h after infection (**Fig. 3b**). We then investigated the correlation between mice survival and the inflammatory response monitored in the lungs 24 h post-infection. In infected IRAP-deficient mice, broncho-alveolar lavage (BAL) fluid contained higher amounts of CXCL1, IL-6, TNF and IL-1 $\beta$  than wild-type mice (**Fig. 3c**). Since AMs are the first innate immune cells to encounter bacteria in the lungs, we isolated AM and tested their cytokine production upon TLR9 and TLR4 stimulation *in vitro*. While a response was barely detectable in AM isolated from wild-type mice, IRAP-deficient AMs secreted substantially higher amounts of all pro-inflammatory cytokines tested upon CpG stimulation (**Fig. 3d**) in comparison to wild-type mice. In contrast, IRAP deficiency did not alter IL-6 and TNF secretion upon LPS stimulation, indicating that the hyper-inflammatory phenotype produced was restricted to TLR9 (**Fig. 3d**).

To control for a potential difference between the two mouse strains in their ability to clear bacteria from the lungs, we measured the pulmonary bacterial load and found it to be identical in IRAP-deficient and wild-type mice (**Fig. 3e**). Consistent with an identical ability of both strains to clear bacteria, *P. aeruginosa* infection led to a similar accumulation of neutrophils and macrophages/monocytes in the airways of both groups (**Supplementary Fig. 2a**). In addition, myeloperoxidase activity that mirrors neutrophil degranulation was similar in BALs from both wild-type and IRAP-deficient mice (**Supplementary Fig. 2b**). Altogether, these

experiments suggest that following *P. aeruginosa* infection, IRAP-deficient mice died earlier probably because of an excessive inflammatory response driven by TLR9 hyper-stimulation.

### **IRAP enzymatic activity is not involved in TLR9 activation**

Our results showed that proper regulation of TLR9 signaling required IRAP. Since IRAP is an aminopeptidase, we wondered if the enzymatic activity of IRAP was involved in the control of TLR9 activation. To investigate this possibility, we tested the effect of an inactive form of IRAP on TLR9 activation. IRAP contains the canonical zinc-binding amino acid motif HELAH, which is essential for the enzymatic activity<sup>26</sup>. A form of IRAP in which the HELAH sequence was changed into HALAH (E465A substitution) co-localized, like the wild-type protein, with syntaxin 6 (Stx6), a SNARE of IRAP<sup>+</sup> endosomes<sup>16,17</sup> (**Fig. 4a**). Both the wild-type and mutated form of IRAP were well expressed, as shown by immunoblotting with anti-IRAP antibodies (**Fig. 4b**) but the mutated form was enzymatically inactive (**Fig. 4c**). When we reconstituted IRAP-deficient BMDCs with wild-type IRAP (**Fig. 4d**) or enzymatically inactive IRAP (**Fig. 4e**), pro-inflammatory cytokine production upon CpG stimulation was similar to wild-type cells. These results demonstrate that the enzymatic activity of IRAP is not involved in the control of TLR9 activation.

### **CpG and TLR9 are cargos of IRAP endosomes**

Since IRAP enzymatic activity was not involved in TLR9 activation, we wondered if IRAP could interfere directly with TLR9 or CpG trafficking. Analysis of CpG-FITC by confocal microscopy demonstrated that CpG strongly colocalized with IRAP. After 20 min of endocytosis, half of the internalized CpG was found in IRAP endosomes, where it was retained for at least 1 h (**Fig. 5a**). Concomitant with IRAP-CpG colocalization, we observed a significant increase of co-localization between IRAP and TLR9-GFP (**Fig. 5b**). While only 20% of TLR9 was found in IRAP endosomes early after CpG stimulation, the TLR9 ligand was a major and persistent cargo of IRAP endosomes.

Since both TLR9 and its ligand trafficked via IRAP endosomes, we wondered if IRAP endosomes overlap with VAMP3, a marker of an endosomal population through which TLR9 traffics towards lysosomes<sup>15</sup>. IRAP, as well as the small GTPase Rab14 and the Q-SNARE Stx6, two others markers of IRAP<sup>+</sup> endosomes in DCs<sup>16,17</sup> coincided with VAMP3 endosomes (**Supplementary Fig. 3**). These results suggest that IRAP endosomes are a new intermediate compartment between early endosomes and the final destination of TLR9, which is the LAMP<sup>+</sup> lysosome. This conclusion is also supported by the absence of colocalization

between IRAP and LAMP that we have shown previously<sup>16,17</sup>.

### **Increased TLR9 lysosomal processing in the absence of IRAP**

Since CpG and TLR9 are cargos of IRAP endosomes, we wondered if IRAP deletion could change the trafficking of CpG and TLR9. Analysis of CpG-FITC trafficking demonstrated that the proportion of TLR9 ligand transported to LAMP<sup>+</sup> vesicles was significantly higher in IRAP-deficient cells than in wild-type cells, an effect that was obvious at early time points (**Fig. 6a**). The accelerated transport to lysosomes of CpG, in IRAP-deficient DCs, was correlated with a change in the intracellular distribution of TLR9-GFP, which was found in lysosomes even in the absence of CpG stimulation (**Fig. 6b**). The presence of TLR9 in the LAMP<sup>+</sup> compartment correlates with proteolytic generation of the active C-terminal fragment of the receptor in DCs and macrophages<sup>7,8,11,12,27</sup>. In agreement with the lysosomal localization of TLR9 in unstimulated IRAP-deficient cells, we found that in IRAP-deficient, but not in wild-type primary mouse embryonic fibroblasts transfected with TLR9-GFP and UNC93B-Cherry, the majority of immunoprecipitated TLR9-GFP corresponded to its processed form (**Fig. 6c**). As expected from the functional assays of TLR stimulation (**Fig. 1a-b**), TLR3 did not colocalize with IRAP and intracellular localization of TLR3 was not affected by IRAP deletion (**Supplementary Fig. 4**). Thus, in the absence of IRAP, TLR9, but not TLR3, was targeted to lysosomes without cell stimulation.

To ensure that the lysosomal expression of TLR9 in IRAP-deficient cells was not the consequence of TLR9-GFP expression by nucleofection, we investigated the localization of endogenous TLR9. Since the only antibody that is specific for TLR9 (**Fig. 6d**) was not sensitive enough to detect TLR9 in whole cell lysate, we isolated early and late phagosomes from wild-type and IRAP-deficient DCs. Although in the absence of CpG, TLR9 was not recruited to phagosomes in wild-type cells, we detected the active C-terminal form of TLR9 in IRAP-deficient late phagosomes. Thus, similar to the TLR9-GFP fusion, endogenous TLR9 was recruited to phagolysosomes without CpG treatment in the absence of IRAP. Intriguingly, when the cells were stimulated with CpG, TLR9 recruitment to early and late phagosomes was identical between wild-type and IRAP-deficient cells (**Fig. 6e**). However, despite the similar recruitment to phagolysosomes of endogenous TLR9 in both wild-type and IRAP-deficient cells upon CpG treatment, TLR9 signaling was exacerbated only in IRAP-deficient cells. This apparent contradiction can be explained by an increased accessibility of TLR9 to CpG in IRAP-deficient cells, suggested by the accelerated translocation of internalized CpG-FITC to lysosomes (**Fig. 6a**). Taken together, these results demonstrate that

the lack of IRAP enhances TLR9 processing.

### **IRAP deletion reduces CpG and TLR9 retention in endosomes**

Since the consequences of IRAP on TLR9 hyperactivation could arise from the properties of IRAP on early endosome trafficking, we wondered if the early steps of CpG and TLR9 trafficking were modified by IRAP depletion. To analyze this, we used the early endosomal antigen, EEA1, a tethering factor known to be involved in homotypic and heterotypic fusion events of early endosomes. EEA1 recruitment to endosome is a mandatory step in endosome maturation and fusion to lysosomes since inhibition of EEA1 activity blocks phagosome maturation<sup>28</sup>. Nevertheless, a fraction of EEA1<sup>+</sup> endosomes displays a slow maturation rate and do not fuse rapidly to late endosomes<sup>29</sup>. To visualize TLR9 and CpG trafficking in EEA1<sup>+</sup> endosomes, we used BMDCs from TLR9-GFP transgenic mice pulsed with CpG-biotin. The uptake of CpG was similar between wild-type and IRAP-deficient BMDCs (**Fig. 7a**), which prompted us to deplete IRAP by lentiviral shRNA (shIRAP) in TLR9-GFP BMDCs (**Fig. 7b**). Colocalization analysis between TLR9-GFP and EEA1 showed that in IRAP-depleted cells, and not in control cells (shNT), TLR9 displayed a vesicular staining in subdomains of EEA1 endosomes in the absence of CpG (**Fig. 7c**, upper panels). Following CpG incubation, the trafficking of CpG was also affected by IRAP depletion. Although in control cells, 25% of internalized CpG remained in EEA1 endosomes for 2 h, in IRAP-depleted cells, CpG was rapidly transferred from EEA1<sup>+</sup> endosomes to TLR9<sup>+</sup> vesicles, (white arrow, **Fig. 7c**). As a consequence of the rapid transfer of CpG to TLR9<sup>+</sup> vesicles in IRAP-depleted cells, the colocalization between CpG and TLR9 was 3 times higher in comparison to control cells (**Fig. 7d**). Thus, IRAP depletion facilitated not only TLR9 processing but also TLR9 access to its ligand.

### **IRAP interacts with FODH4 formin**

Altogether, these results highlighted a role for IRAP in TLR9 and CpG retention in EEA1<sup>+</sup> endosomes that was independent on its enzymatic activity. We reasoned that the effect of IRAP on TLR9 activation could be mediated by interactions with cytosolic proteins. Two cytoskeleton factors have been previously identified to interact with the cytosolic domain of IRAP: vimentin<sup>19</sup> and FHOD1 (formin homology domain-containing proteins; synonym: FHOS-formin homologue overexpressed in the spleen)<sup>20</sup>. Vimentin forms intermediate filaments, cytoskeleton components that are important for anchoring intracellular organelles<sup>30</sup>. FHOD formins are actin polymerization factors and are involved in anchoring vesicles to

the actin cytoskeleton<sup>31</sup>. Thus, vimentin and formins could play a role in the control of IRAP-mediated trafficking of TLR9. Proximity ligation and co-immunoprecipitation experiments in fibroblasts and in DCs failed to show a robust interaction between IRAP and vimentin (data not shown), which implies that the IRAP-vimentin interaction that has been demonstrated in adipocytes<sup>19</sup> might be specific to that cell type.

To investigate the FHOD1-IRAP interaction in DCs, we first explored the expression of FHOD1 in different cell types as reported in the gene expression database of the ImmGen<sup>32</sup> consortium (**Fig. 8a**). The mRNA expression data recovered from ImmGen (<https://www.immgen.org/Databrowserpage.swf>) showed that while FHOD1 expression is restricted to a subset of macrophages, FHOD4, a formin from the same family, has a wider distribution and higher expression in monocytes and DCs. As a consequence, we tested the interaction between IRAP and FHOD4. Endogenous FHOD4, as well as a FHOD4-GFP fusion protein interacted with IRAP as demonstrated by reciprocal co-immunoprecipitations (**Fig. 8b** and **Supplementary Fig. 5a**) and by proximity ligation assay *in situ*<sup>23</sup> (**Fig. 8c** and **Supplementary Fig. 5b**). Confocal microscopy showed that FHOD4 could be recruited to IRAP<sup>+</sup> endosomes, together with a vesicular actin coat labeled by phalloidin (**Fig. 8d**). These results suggested that FHOD4 could anchor IRAP<sup>+</sup> endosomes to the actin cytoskeleton.

To investigate if FHOD4-IRAP interaction was involved in TLR9 activation in DCs, we knocked-down FHOD4 in BMDCs from TLR9-GFP transgenic mice. FHOD4 was reproducibly reduced by 95% ( $\pm$  10%) in the cells transduced with two shRNA (17 and 20) targeting FHOD4 (**Fig. 8e**). In the absence of FHOD4 and CpG stimulation, 40% ( $\pm$  5%) of the endogenous TLR9-GFP was found in the cleaved form (**Fig. 8f**). In agreement with the increased basal processing of TLR9-GFP, the GFP-fused TLR9 was found in lysosomes in FHOD4 depleted cells (**Fig. 8g**). Thus, TLR9 trafficking and processing were affected by FHOD4 depletion, like in the case of IRAP deletion.

Considering the impact of FHOD4 depletion on TLR9 localization, we expected to have an increased TLR9-driven inflammatory response in FHOD4 depleted BMDCs. When incubated with CpG, FHOD4 depleted cells (wt-shFHOD4) secreted significantly more pro-inflammatory cytokines than the cells transduced with a non-targeting shRNA (wt-shNT) (**Fig. 8h** and **Supplementary Fig. 6a**). Consistent with low expression of FHOD1 in BMDCs (**Supplementary Fig. 6b**), its depletion did not affect TLR9-GFP localization or activation (**Supplementary Fig. 6c-d**). These results suggest that IRAP anchors endosomal vesicles to the actin cytoskeleton through its specific interaction with FHOD4, slowing their transport to lysosomes (**Supplementary Fig. 7**). A major effect of these molecular interactions is

ensuring a limited interaction between TLR9 and its ligand, which prevents hyperinflammation.

## DISCUSSION

Recognition of host nucleic acids by intracellular TLRs is a risk for autoimmunity. For example, inappropriate activation of endosomal TLRs by self DNA has a major role in inflammation that occurs in systemic lupus erythematosus, arthritis and psoriasis<sup>33</sup>. To avoid hyperactivation of TLRs, their encounter with the ligands and ability to signal must be tightly regulated. TLR9, like other intracellular TLRs, exits ER by interacting with Unc93b<sup>34</sup>. Unlike other TLRs, the TLR9-Unc93b complex reaches the cell surface and is later internalized into a poorly characterized endosomal compartment through AP-2 mediated endocytosis<sup>6</sup>.

In this study, we identified IRAP as a regulator of CpG and TLR9 intracellular trafficking and *in vivo* activation of TLR9. IRAP deficiency led to the rapid transport of internalized CpG to lysosomes and to TLR9 localization in lysosomes, where TLR9 is cleaved into its active C-terminal form in the absence of CpG ligand. We observed this aberrant TLR9 trafficking and processing not only for TLR9-GFP, but also for endogenous TLR9 detected with anti-TLR9 antibodies. Lysosomal localization of TLR9 in IRAP-deficient cells might be a consequence of accelerated trafficking of its ligand, which normally is retained in IRAP<sup>+</sup> endosomes for a long time. The aberrant trafficking of both the ligand and the receptor led to an uncontrolled inflammatory response to TLR9 ligands, which culminated with animal death following an infection with *P. aeruginosa*, a bacterium sensed by TLR9<sup>25</sup>. Altogether, our results show that IRAP is required to avoid excessive TLR9-driven inflammatory responses. In view of these results, it is conceivable that IRAP plays a role in human autoimmune pathologies through its effects on TLR9 signaling. The recent identification of a genetic association between psoriasis, one of the autoimmune disorders implicating TLR9 activation, and a nonsense mutation in the *Lnpep* gene encoding IRAP is consistent with this hypothesis<sup>21</sup>.

Our colocalization experiments define an endosomal compartment that is described by the presence of IRAP, Rab14 and Stx6 and partially overlaps with VAMP3<sup>+</sup> and EEA1<sup>+</sup> endosomes. VAMP3 and TLR9 have been shown to co-localize in an intermediate step of the route that TLR9 follows towards lysosomes and which depends on the AP-3 adaptor<sup>15</sup>. Our data suggest that IRAP delays the trafficking of CpG and TLR9 from EEA1<sup>+</sup> endosomes to lysosomes, with important functional consequences. To understand how IRAP could mechanistically affect the dynamics of the early endosomal compartment in which CpG and

TLR9 are retained, we screen for cytoskeletal proteins that might interact with IRAP and could interfere with endosomal motility. Indeed, considering that the cytosolic tail of IRAP was shown to interact with two cytoskeleton components, an actin nucleation factor, the formin FHOD1<sup>20</sup> and the intermediate filament vimentin<sup>19</sup>, we hypothesized that these interactions ensure the anchoring of IRAP and TLR9 endosomes to cytoskeleton. Whereas the interaction of IRAP with vimentin was not detectable in DCs (experiments not shown), we found that IRAP binds to FHOD4 formin.

Formins are major actin nucleation factors that drive the assembly of actin monomers into filamentous structures and remain associated with the barbed end during filament elongation<sup>35</sup>. A knock-down of FHOD4 had effects similar to IRAP deletion on TLR9 trafficking and the cellular response to CpG. These results suggest that by promoting actin assembly on endosomes, FHOD4 prevents the transfer of endosomes to microtubules, delaying their retrograde transport towards lysosomes, as reported for the formin mDia1<sup>36</sup>. Actin polymerization around the endosomal vesicles containing TLR9 ligands has been shown to be also driven by the other key actin nucleation factor, Arp2/3, and to be essential in limiting TLR9 signaling<sup>37</sup>. Both, FHOD4 and Arp2/3 are activated by the same small GTPase of Rho family, Cdc42<sup>35</sup>, suggesting that these two actin-remodeling factors might cooperate in the regulation of TLR9 signaling, like they cooperate in phagocytic cup formation<sup>38</sup>.

The intervention of FHOD4 in interaction with IRAP for modulating TLR9 function has implications for potential links between extracellular stimuli, such as cytokines and the ability of TLR9 to respond to its ligands. It has been previously reported that TLR responses can be inhibited by extracellular stimuli such as cytokines<sup>39</sup> or integrin ligation<sup>40,41</sup>. Since Cdc42 activation occurs downstream integrin, receptor tyrosine kinase or G-protein-coupled receptors signaling<sup>42</sup>, it could affect actin polymerization and the anchoring of CpG<sup>+</sup>-TLR9<sup>+</sup> endosomes by IRAP. Thus, the anchoring of CpG<sup>+</sup>-TLR9<sup>+</sup> endosomes to actin cytoskeleton could be essential in regulating TLR9 dependent cellular responses to the environment.

## ACKNOWLEDGEMENTS

We are grateful to N. Goudin and S. Benadda for advice on analysis and quantification of confocal microscopy images, to S. Keller for anti-IRAP rabbit antibodies and mice, to D. Billadeau for anti-FHODs antibodies and to F. Benvenuti, F. Perez and S. Blystone for plasmid vectors. This work received financial support from the French “Agence Nationale de Recherche”, ANR IRAPDC, ANR-15-CE15-0005 to L.S, ANR 2010 MIDI 008 01 to B.M,

ANR post-doctoral support to D. D, FRM PhD fellowship to A.C.A.A, an Institut Curie Ph.D. fellowship to M. T and the Initiative and Networking Fund of the Helmholtz Association (VH-NG-637) to M.M.B. We thank the Foundation “ARC pour la Recherche sur le cancer” for the acquisition of Leica SP8 confocal microscope and for the financial support to J.B and S.M.

### **COMPETING FINANCIAL INTERESTS**

The authors declare no competing financial interests.

### **AUTHOR CONTRIBUTIONS**

J.B, D.D, C.A.A.A, M.T, S.M, I.E, L.R.V, M.D.L, F.M, B.M and L.S designed, did the experiments and analyzed the data. M.G.T contributed to confocal images acquisition and analysis. M.M.B and M.C contributed to new reagents or analytic tools. B.M and L.S wrote the paper, supervised the project and edited the paper.

## References

- 1 Lee, B. L. & Barton, G. M. Trafficking of endosomal Toll-like receptors. *Trends in cell biology* **24**, 360-369, doi:10.1016/j.tcb.2013.12.002 (2014).
- 2 Latz, E. *et al.* TLR9 signals after translocating from the ER to CpG DNA in the lysosome. *Nat Immunol* **5**, 190-198, doi:10.1038/ni1028 (2004).
- 3 Leifer, C. A. *et al.* TLR9 is localized in the endoplasmic reticulum prior to stimulation. *J Immunol* **173**, 1179-1183 (2004).
- 4 Fukui, R. *et al.* Unc93B1 restricts systemic lethal inflammation by orchestrating Toll-like receptor 7 and 9 trafficking. *Immunity* **35**, 69-81, doi:10.1016/j.immuni.2011.05.010 (2011).
- 5 Garcia-Cattaneo, A. *et al.* Cleavage of Toll-like receptor 3 by cathepsins B and H is essential for signaling. *Proc Natl Acad Sci U S A* **109**, 9053-9058, doi:10.1073/pnas.1115091109 (2012).
- 6 Lee, B. L. *et al.* UNC93B1 mediates differential trafficking of endosomal TLRs. *Elife* **2**, e00291, doi:10.7554/eLife.00291 (2013).
- 7 Asagiri, M. *et al.* Cathepsin K-dependent toll-like receptor 9 signaling revealed in experimental arthritis. *Science* **319**, 624-627, doi:10.1126/science.1150110 (2008).
- 8 Ewald, S. E. *et al.* Nucleic acid recognition by Toll-like receptors is coupled to stepwise processing by cathepsins and asparagine endopeptidase. *J Exp Med* **208**, 643-651, doi:10.1084/jem.20100682 (2011).
- 9 Hipp, M. M. *et al.* Processing of human toll-like receptor 7 by furin-like proprotein convertases is required for its accumulation and activity in endosomes. *Immunity* **39**, 711-721, doi:10.1016/j.immuni.2013.09.004 (2013).
- 10 Maschalidi, S. *et al.* Asparagine endopeptidase controls anti-influenza virus immune responses through TLR7 activation. *PLoS Pathog* **8**, e1002841, doi:10.1371/journal.ppat.1002841 (2012).
- 11 Park, B. *et al.* Proteolytic cleavage in an endolysosomal compartment is required for activation of Toll-like receptor 9. *Nat Immunol* **9**, 1407-1414, doi:10.1038/ni.1669 (2008).
- 12 Sepulveda, F. E. *et al.* Critical role for asparagine endopeptidase in endocytic Toll-like receptor signaling in dendritic cells. *Immunity* **31**, 737-748, doi:10.1016/j.immuni.2009.09.013 (2009).
- 13 Hayashi, K., Sasai, M. & Iwasaki, A. Toll-like receptor 9 trafficking and signaling for type I interferons requires PIKfyve activity. *International immunology* **27**, 435-445, doi:10.1093/intimm/dxv021 (2015).
- 14 Hazeki, K., Uehara, M., Nigorikawa, K. & Hazeki, O. PIKfyve regulates the endosomal localization of CpG oligodeoxynucleotides to elicit TLR9-dependent cellular responses. *PLoS One* **8**, e73894, doi:10.1371/journal.pone.0073894 (2013).
- 15 Sasai, M., Linehan, M. M. & Iwasaki, A. Bifurcation of Toll-like receptor 9 signaling by adaptor protein 3. *Science* **329**, 1530-1534, doi:10.1126/science.1187029 (2010).
- 16 Saveanu, L. *et al.* IRAP identifies an endosomal compartment required for MHC class I cross-presentation. *Science* **325**, 213-217, doi:10.1126/science.1172845 (2009).
- 17 Weimershaus, M. *et al.* Conventional dendritic cells require IRAP-Rab14 endosomes for efficient cross-presentation. *J Immunol* **188**, 1840-1846, doi:10.4049/jimmunol.1101504 (2012).
- 18 Hosaka, T. *et al.* p115 Interacts with the GLUT4 vesicle protein, IRAP, and plays a critical role in insulin-stimulated GLUT4 translocation. *Mol Biol Cell* **16**, 2882-2890, doi:10.1091/mbc.E05-01-0072 (2005).
- 19 Hirata, Y. *et al.* Vimentin binds IRAP and is involved in GLUT4 vesicle trafficking. *Biochem Biophys Res Commun* **405**, 96-101, doi:10.1016/j.bbrc.2010.12.134 (2011).
- 20 Tojo, H. *et al.* The Formin family protein, formin homolog overexpressed in spleen,

- interacts with the insulin-responsive aminopeptidase and profilin IIa. *Mol Endocrinol* **17**, 1216-1229, doi:10.1210/me.2003-0056 (2003).
- 21 Cheng, H. *et al.* Identification of a missense variant in LNPEP that confers psoriasis risk. *J Invest Dermatol* **134**, 359-365, doi:10.1038/jid.2013.317 (2014).
- 22 Stow, J. L., Low, P. C., Offenhauser, C. & Sangermani, D. Cytokine secretion in macrophages and other cells: pathways and mediators. *Immunobiology* **214**, 601-612, doi:10.1016/j.imbio.2008.11.005 (2009).
- 23 Leuchowius, K. J., Weibrecht, I. & Soderberg, O. In situ proximity ligation assay for microscopy and flow cytometry. *Curr Protoc Cytom* **Chapter 9**, Unit 9 36, doi:10.1002/0471142956.cy0936s56 (2011).
- 24 Greene, C. M. *et al.* TLR-induced inflammation in cystic fibrosis and non-cystic fibrosis airway epithelial cells. *J Immunol* **174**, 1638-1646 (2005).
- 25 Benmohamed, F. *et al.* Toll-Like Receptor 9 Deficiency Protects Mice against *Pseudomonas aeruginosa* Lung Infection. *PLoS One* **9**, e90466, doi:10.1371/journal.pone.0090466 (2014).
- 26 Saveanu, L. & van Endert, P. The role of insulin-regulated aminopeptidase in MHC class I antigen presentation. *Front Immunol* **3**, 57, doi:10.3389/fimmu.2012.00057 (2012).
- 27 Onji, M. *et al.* An essential role for the N-terminal fragment of Toll-like receptor 9 in DNA sensing. *Nat Commun* **4**, 1949, doi:10.1038/ncomms2949 (2013).
- 28 Fratti, R. A., Backer, J. M., Gruenberg, J., Corvera, S. & Deretic, V. Role of phosphatidylinositol 3-kinase and Rab5 effectors in phagosomal biogenesis and mycobacterial phagosome maturation arrest. *J Cell Biol* **154**, 631-644, doi:10.1083/jcb.200106049 (2001).
- 29 Lakadamyali, M., Rust, M. J. & Zhuang, X. Ligands for clathrin-mediated endocytosis are differentially sorted into distinct populations of early endosomes. *Cell* **124**, 997-1009, doi:10.1016/j.cell.2005.12.038 (2006).
- 30 Kim, S. & Coulombe, P. A. Intermediate filament scaffolds fulfill mechanical, organizational, and signaling functions in the cytoplasm. *Genes Dev* **21**, 1581-1597, doi:10.1101/gad.1552107 (2007).
- 31 Goode, B. L. & Eck, M. J. Mechanism and function of formins in the control of actin assembly. *Annu Rev Biochem* **76**, 593-627, doi:10.1146/annurev.biochem.75.103004.142647 (2007).
- 32 Heng, T. S. & Painter, M. W. The Immunological Genome Project: networks of gene expression in immune cells. *Nat Immunol* **9**, 1091-1094, doi:10.1038/ni1008-1091 (2008).
- 33 Rifkin, I. R., Leadbetter, E. A., Busconi, L., Viglianti, G. & Marshak-Rothstein, A. Toll-like receptors, endogenous ligands, and systemic autoimmune disease. *Immunological reviews* **204**, 27-42, doi:10.1111/j.0105-2896.2005.00239.x (2005).
- 34 Brinkmann, M. M. *et al.* The interaction between the ER membrane protein UNC93B and TLR3, 7, and 9 is crucial for TLR signaling. *J Cell Biol* **177**, 265-275, doi:10.1083/jcb.200612056 (2007).
- 35 Kuhn, S. & Geyer, M. Formins as effector proteins of Rho GTPases. *Small GTPases* **5**, e29513, doi:10.4161/sgtp.29513 (2014).
- 36 Fernandez-Borja, M., Janssen, L., Verwoerd, D., Hordijk, P. & Neefjes, J. RhoB regulates endosome transport by promoting actin assembly on endosomal membranes through Dial1. *Journal of cell science* **118**, 2661-2670, doi:10.1242/jcs.02384 (2005).
- 37 Prete, F. *et al.* Wiskott-Aldrich syndrome protein-mediated actin dynamics control type-I interferon production in plasmacytoid dendritic cells. *J Exp Med* **210**, 355-374, doi:10.1084/jem.20120363 (2013).
- 38 Seth, A., Otomo, C. & Rosen, M. K. Autoinhibition regulates cellular localization and actin assembly activity of the diaphanous-related formins FRLalpha and mDial1. *J Cell*

- Biol* **174**, 701-713, doi:10.1083/jcb.200605006 (2006).
- 39 Wimmer, N. *et al.* Lymphotoxin beta receptor activation on macrophages induces cross-tolerance to TLR4 and TLR9 ligands. *J Immunol* **188**, 3426-3433, doi:10.4049/jimmunol.1103324 (2012).
- 40 Acharya, M. *et al.* alphav Integrins combine with LC3 and atg5 to regulate Toll-like receptor signalling in B cells. *Nat Commun* **7**, 10917, doi:10.1038/ncomms10917 (2016).
- 41 Han, C. *et al.* Integrin CD11b negatively regulates TLR-triggered inflammatory responses by activating Syk and promoting degradation of MyD88 and TRIF via Cbl-b. *Nat Immunol* **11**, 734-742, doi:10.1038/ni.1908 (2010).
- 42 Etienne-Manneville, S. Cdc42--the centre of polarity. *Journal of cell science* **117**, 1291-1300, doi:10.1242/jcs.01115 (2004).

## Figure Legends

### Figure 1. IRAP deletion increases TLR9 response

(a) Wild-type (WT) and IRAP-deficient (KO) BMDCs were stimulated with different TLR ligands for 16 h and the secretion of IL-6, IL-12(p40) and TNF in supernatants was measured by ELISA (n=3 experiments, mean  $\pm$  SEM, \* p<0.03, \*\* p<0.006). (b) WT and KO BMDCs were incubated for 16 h with TLR ligands and IFN- $\beta$  was measured by ELISA (n=3 experiments, \*p<0.03, \*\*p<0.0009). (c-d) Splenic cDCs (c) or pDCs (d) from WT and KO mice were isolated by cell sorting (c) or anti-PDCA-1 magnetic beads (d), incubated overnight with CpG-B or CpG-A and cytokine secretion was measured by ELISA (n=2 experiments, mean  $\pm$  SEM, \*p<0.001, \*\*p<0.0008). (e) WT and KO BMDCs were incubated for 3 h with CpG-B or LPS and mRNA for TNF, IL-6 and IL-12 was quantified by RT-PCR using as reporters GAPDH and HPRT1. NS= non-stimulated cells. (n= 4 experiments, mean  $\pm$  SEM, \* p<0.05). (f) mRNAs for IL-6 and IL-12 from WT and KO splenic pDCs, stimulated or not (NS) with CpG-B, were measured by RT-PCR using the same reporter genes as in e (n= 3 experiments, mean  $\pm$  SEM, \* p<0.022). See also **Supplementary Fig. 1**.

### Figure 2. Increased TLR9 signaling in IRAP-deficient DCs

Proximity ligation assay (PLA) for detection of MyD88-NF- $\kappa$ B (a) or MyD88-IRF7 (b) proximity was performed with specific antibodies against MyD88, NF- $\kappa$ B and IRF7. The graphs show the quantification of MyD88 interaction with NF- $\kappa$ B (a) or IRF7 (b) by PLA. (n=3 experiments, mean  $\pm$  SEM, \*p<0.01, \*\*p<0.004). Statistical analysis was performed with Student t test. (c-d) WT or KO BMDCs were incubated with TLR ligands (CpG-B: 10  $\mu$ g/ml, LPS: 100 ng/ml) for 10, 20, 30, 40, 60 and 120 minutes. Cells lysates were assessed for ERK (c) and I-KB- $\alpha$  (d) phosphorylation by immunoblot and ELISA. Total ERK (t-ERK) and I-KB- $\alpha$  (t-I-KB- $\alpha$ ) were also measured. Phosphorylated ERK (p-ERK) proteins were quantified and normalized over total ERK (t-ERK) using IMAGE J software. (c, d, n= 3 experiments, mean  $\pm$  SD, c, \* p<0.01, \*\* p<0.009, \*\*\* p<0.002, d, \*p<0.01, \*\*p<0.009, \*\*\*p<0.002).

### Figure 3. IRAP-deficient mice display a hyper-inflammatory phenotype driven by TLR9 activation

(a) IL-6 production was measured in serum of WT or KO mice 2 h after i.v. injection of CpG-B (left panel) or LPS (right panel) (n=9 animals, mean  $\pm$  SEM, \* p<0.001). (b) WT and KO

mice (n=9 in each group), were inoculated intranasally with *P. Aeruginosa* at  $10^6$  CFU/mouse. Animal survival was determined up to 7 days post-infection (n=9 mice, \* p<0.02). (c) Broncho-alveolar lavage (BAL) fluid levels of CXCL1, IL-6, TNF and IL-1 $\beta$  in WT and KO mice 24 h after intranasal inoculation of *P. Aeruginosa* ( $10^6$  CFU/mice) (n=9 animals, mean  $\pm$  SEM \* p<0.05). (d) TNF, CXCL1 and IL-6 secretion in supernatants of non-stimulated (NS), CpG-B- or LPS-stimulated WT or KO alveolar macrophages (2 independent experiments, mean  $\pm$  SEM, \* p<0.05). (e) Twenty-four hours post-infection, bacterial load was determined in lungs from WT and KO mice (n=10 animals). See also **Supplementary Fig. 2**.

#### **Figure 4. IRAP enzymatic activity is not involved in TLR9 activation**

(a) KO BMDCs reconstituted with active or inactive IRAP-HA by nucleofection were seeded on fibronectin-coated slides and stained with anti-Stx6 and anti-HA specific antibodies. The graph shows the colocalization between IRAP and Stx6 (n=10 cells, mean  $\pm$  SEM). (b) IRAP-deficient fibroblasts were transfected by electroporation with active or inactive IRAP and 36 h later, IRAP expression was analyzed by immunoblotting with anti-IRAP antibodies. (c) IRAP was immunoprecipitated with anti-IRAP antibodies from the fibroblasts transfected as in (b) and the aminopeptidase activity was tested by incubation of the beads with the colorimetric substrate Leu-AMC (3 independent experiments, mean $\pm$  SEM). (d-e) IRAP-deficient BMDCs reconstituted with active (d) or inactive (e) IRAP were stimulated with TLR ligands for 16 h and IL-6 secretion was measured by ELISA (three (d) or two (e) independent experiments, mean  $\pm$  SEM, \*p<0.015, \*\*p<0.002, \*\*\*p<0.0011).

#### **Figure 5. CpG and TLR9 are cargo of IRAP endosomes**

(a) WT BMDCs were pulsed for 20 minutes with CpG-FITC, chased at 37°C for the indicated time-points, washed in PBS, fixed and stained with anti-IRAP and anti-FITC specific antibodies (n=8 cells, mean  $\pm$  SEM, \*p<0.012, \*\*p<0.0001). (b) WT BMDCs were transfected with TLR9-GFP by nucleofection. Two days later, the cells were stimulated or not with CpG-B for 20 min, fixed and stained with anti-IRAP specific antibodies (n=10 cells, mean  $\pm$  SEM, \*p<0.0002). See also **Supplementary Fig. 3**.

#### **Figure 6. IRAP absence increases the susceptibility of TLR9 to lysosomal processing**

(a) WT and KO BMDCs were pulsed for 20 minutes with CpG-FITC, chased at 37°C for the indicated time-points, washed in PBS, fixed and stained with anti-LAMP1 and anti-FITC

specific antibodies (n= 8 cells, mean  $\pm$  SEM, \*p<0.013, \*\*p<0.0001). (b) KO and WT BMDCs were transfected with TLR9-GFP by nucleofection and 48 h later stimulated or not with CpG-B for 20 or 120 min. The cells were fixed and stained with specific antibodies for LAMP1 (n= 8 cells, mean  $\pm$  SEM, \*p<0.02, \*\*p<0.0012). (c) WT and KO fibroblasts expressing TLR9-GFP and Unc93b-Cherry were lysed in 1% NP-40 and TLR9-GFP was immunoprecipitated with anti-GFP antibodies and analyzed by anti-GFP immunoblot. The graph represents the quantification of GFP immunoblots (n= 3 experiments, mean  $\pm$  SEM, \*p<0.0067). Phagosomes from *Tlr9*<sup>-/-</sup> (TLR9-ko, d), WT and KO (e) BMDCs unstimulated or stimulated with CpG-B (10  $\mu$ g/ml) were magnetically purified after 20 min or 120 min. Proteins expressed in phagosomes (10  $\mu$ g) were resolved by SDS-PAGE and endogenous TLR9 and LAMP1 proteins were visualized by immunoblot. Shown is a representative example of two independent experiments.

#### **Figure 7. IRAP deletion reduces CpG and TLR9 retention in early endosomes**

(a) CpG-FITC up-take by WT and KO BMDCs was measured by flow cytometry. (b-c) BMDCs from TLR9-GFP transgenic mice were transduced with a lentivirus coding for a shRNA against IRAP (shIRAP) or a non-targeting shRNA (shNT). (b) The efficiency of IRAP knockdown was analyzed by immunoblotting, using anti-IRAP antibodies and anti  $\alpha$ -Tubulin antibodies for the loading control. (c) The cells were pulsed or not with Biotinylated-CpG, washed and chased for the indicated time points. After fixation, the cells were stained with anti-EEA1 specific antibodies. (d) The graphs represent the percentage of colocalization between the proteins visualized in (c) (n=10 cells, \*p<0.013, \*\*p<0.002, \*\*\*p<0.0001).

#### **Figure 8. IRAP interacts with FODH4 formin**

(a) IRAP (encoded by *Lnpep* gene), FHOD1 (encoded by *Fhod1* gene), FHOD4 (encoded by *Fmnl1* gene) and TLR9 mRNA expression data were recovered from immgen (<https://www.immgen.org/Databrowserpage.swf>) for pDCs, monocytes and red pulp spleen macrophages. (b) Endogenous IRAP and FHOD4 were immunoprecipitated with antibodies anti-IRAP and anti-FHOD4 respectively and the precipitates were split in two and analyzed by immunoblot as indicated (TCL= total cell lysate). (c) *In situ* IRAP-FHOD4 interaction was detected by PLA using antibodies against IRAP and FHOD4 (n=10 cells). (d) WT fibroblasts expressing FHOD4-GFP were fixed and stained with phalloidin and anti-IRAP antibodies. 40% (+/-5) of IRAP colocalized with FHOD4 (n=10 cells, mean  $\pm$  SEM). (e-g) BMDCs from

TLR9-GFP transgenic mice were transduced with two lentiviruses coding for shRNAs against FHOD4 (shFHOD4 17 and shFHOD4 20) or a non-targeting shRNA (shNT). (e) The efficiency of FHOD4 knock-down was analyzed by immunoblotting using anti FHOD4 antibodies. (f) Endogenous TLR9-GFP processing in cells transduced with shNT or shFHOD4 (20) was analyzed by immunoblot with anti-GFP antibodies. (g) Endogenous TLR9-GFP localization was analyzed by confocal microscopy using an anti-LAMP1 antibody. The graph represents the quantification of TLR9-GFP-LAMP1 colocalization (n=10 cells, mean  $\pm$  SEM , \*p<0.002). (h) WT and KO BMDCs were transduced with shNT and shFHOD4 (20) lentiviruses and stimulated with TLR ligands for 6 h. The secretion of IL- 12p40 in supernatants was measured by ELISA (n=3 experiments, mean  $\pm$  SEM, \*p<0.017). See also **Supplementary Fig. 5-6**.

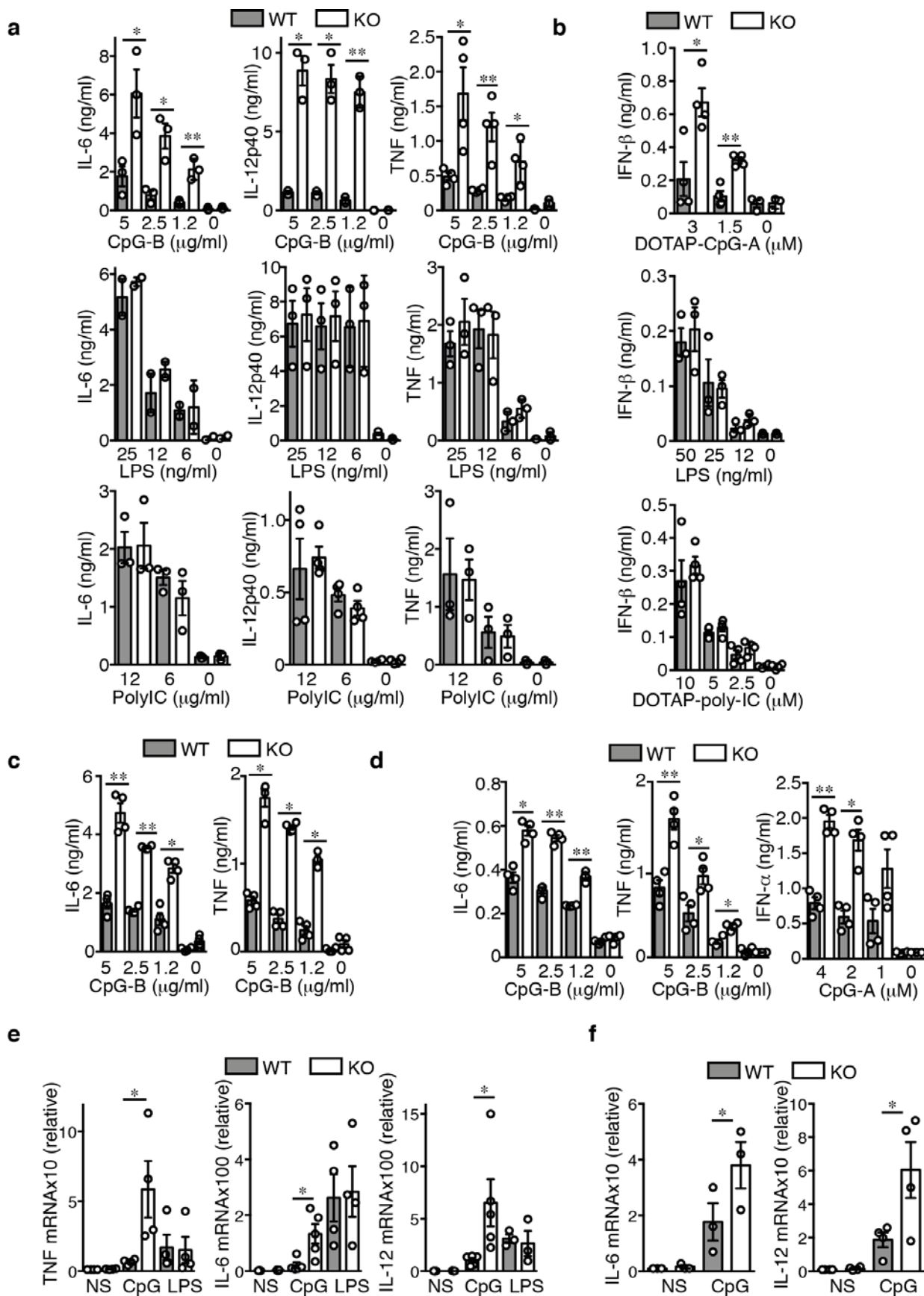


Figure 1

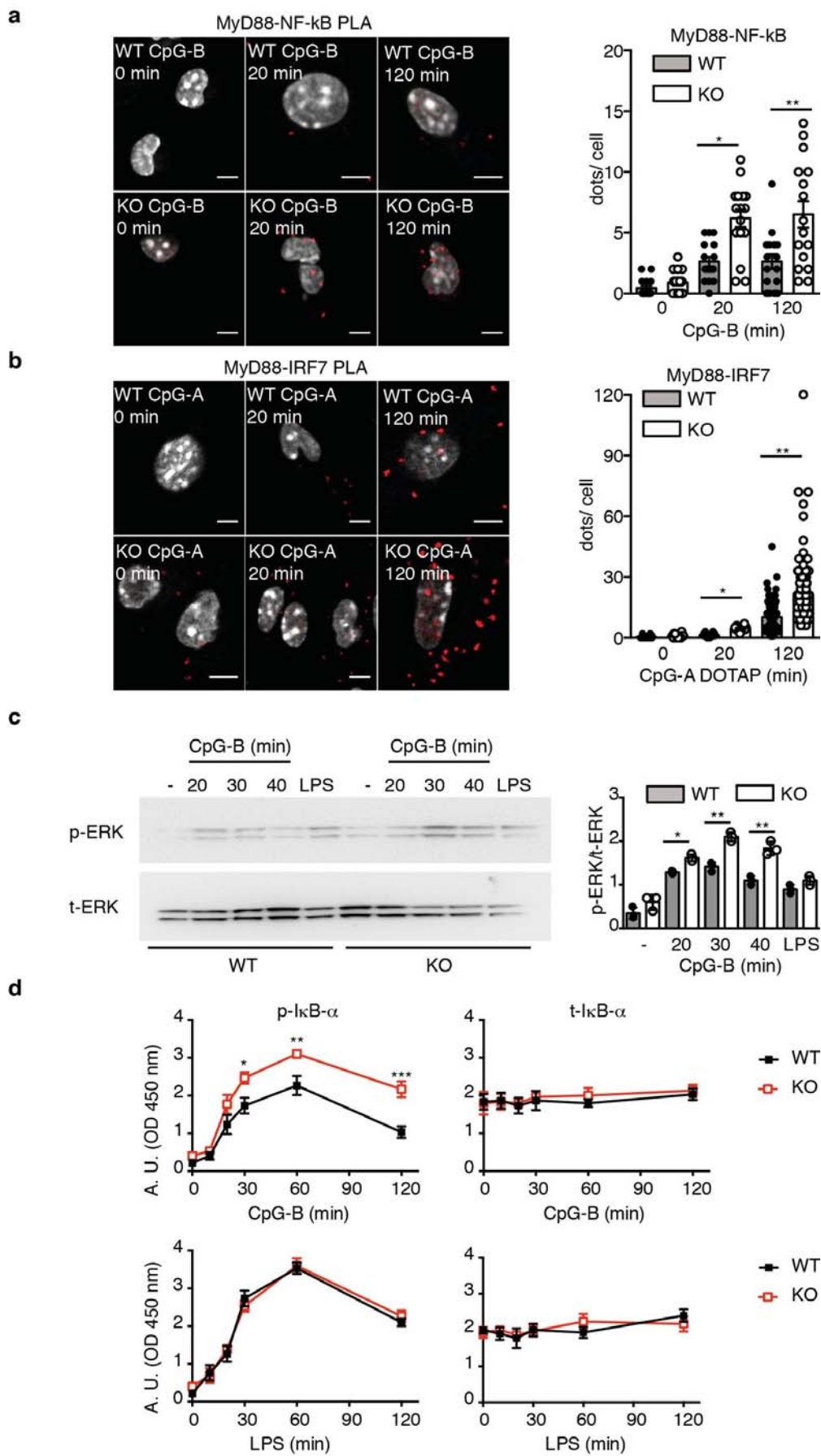


Figure 2

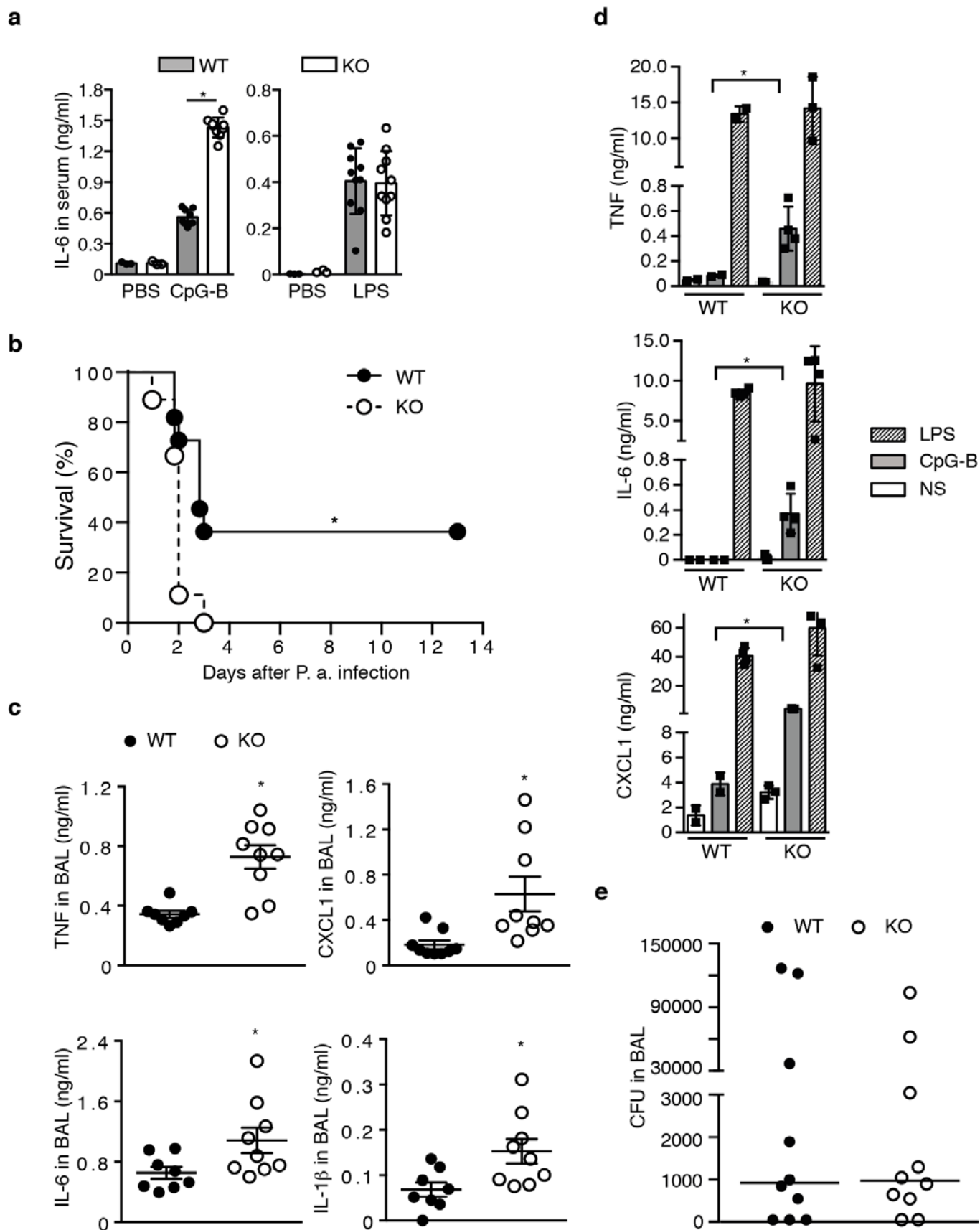


Figure 3

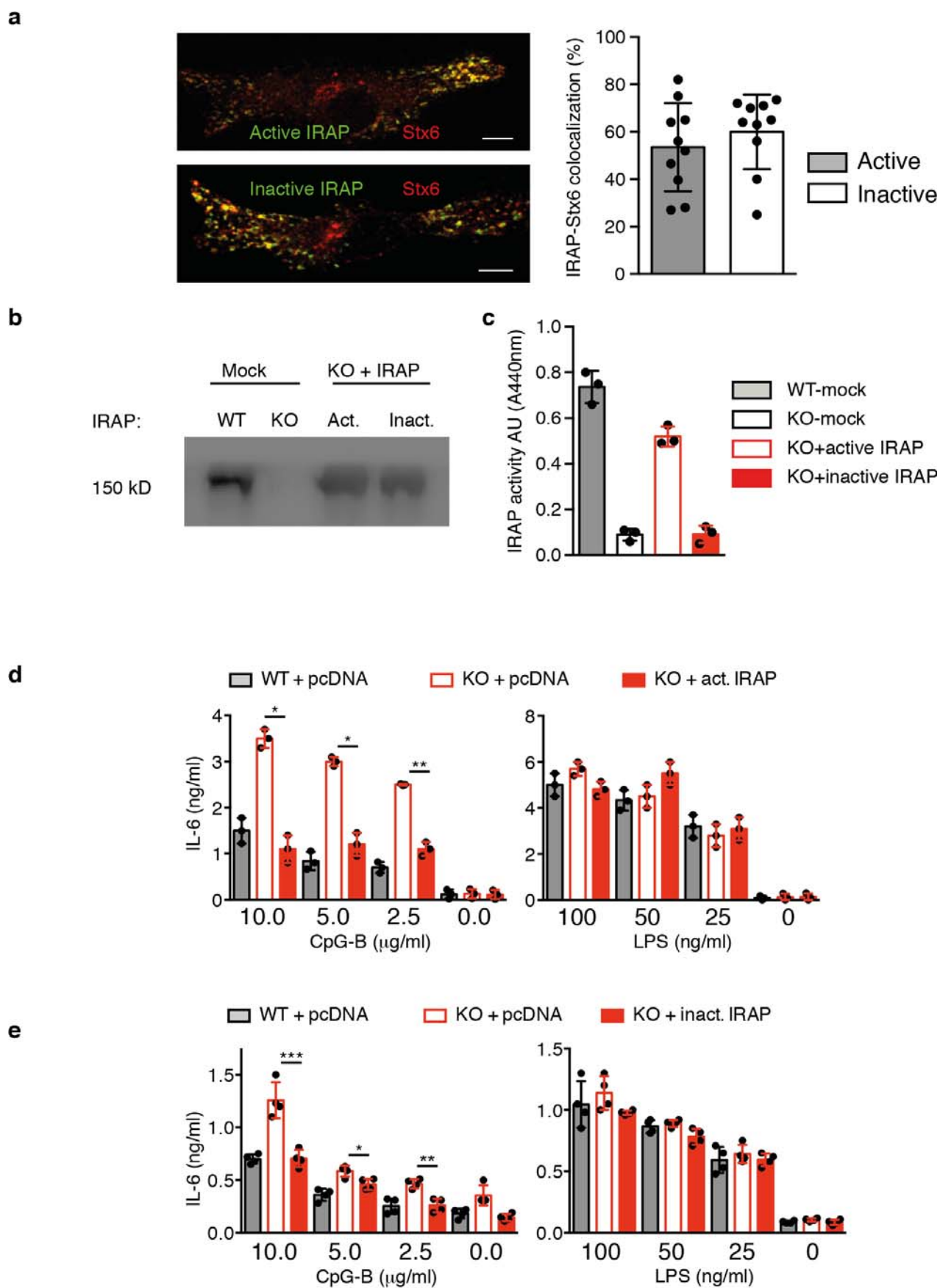


Figure 4

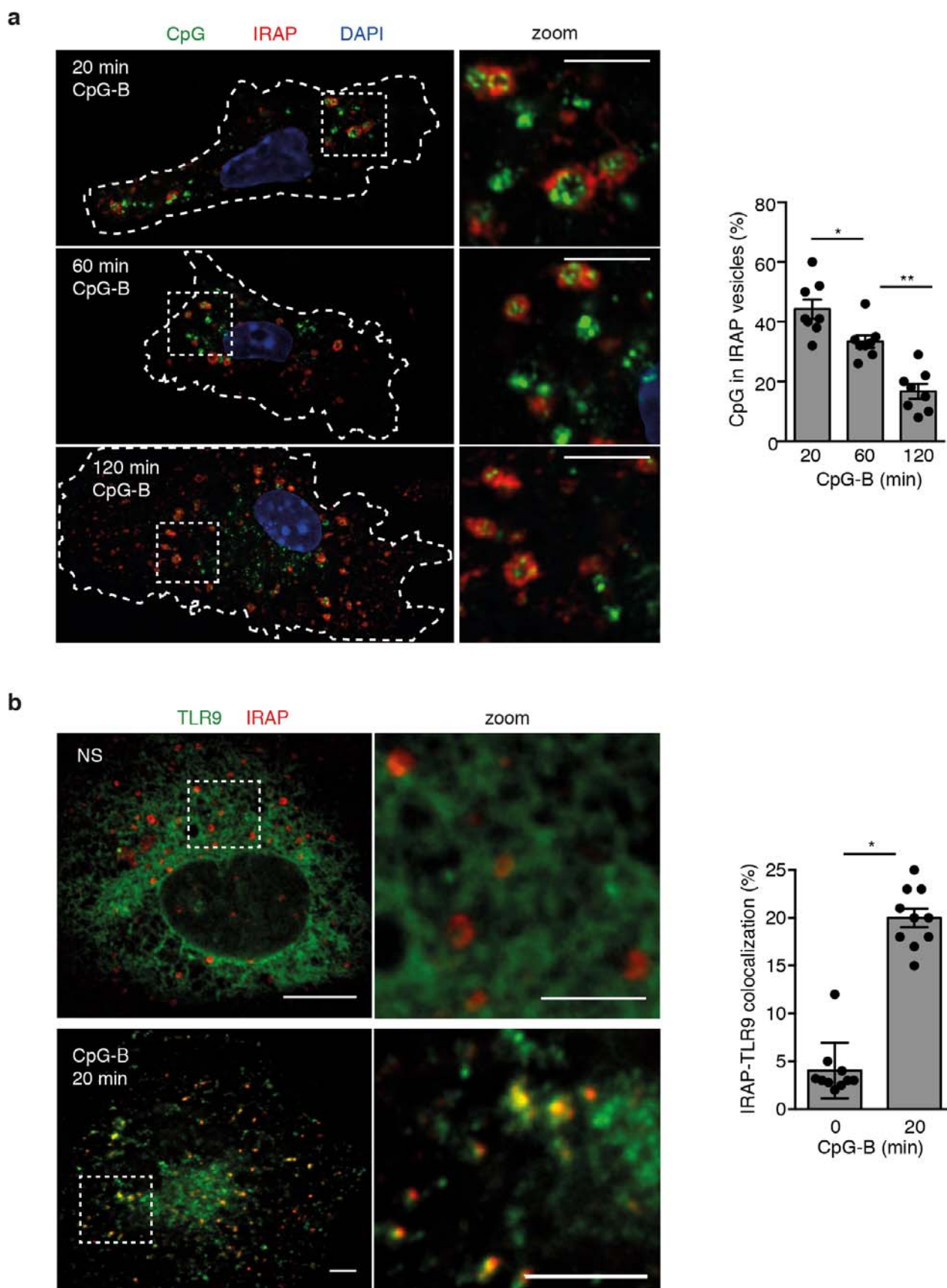


Figure 5

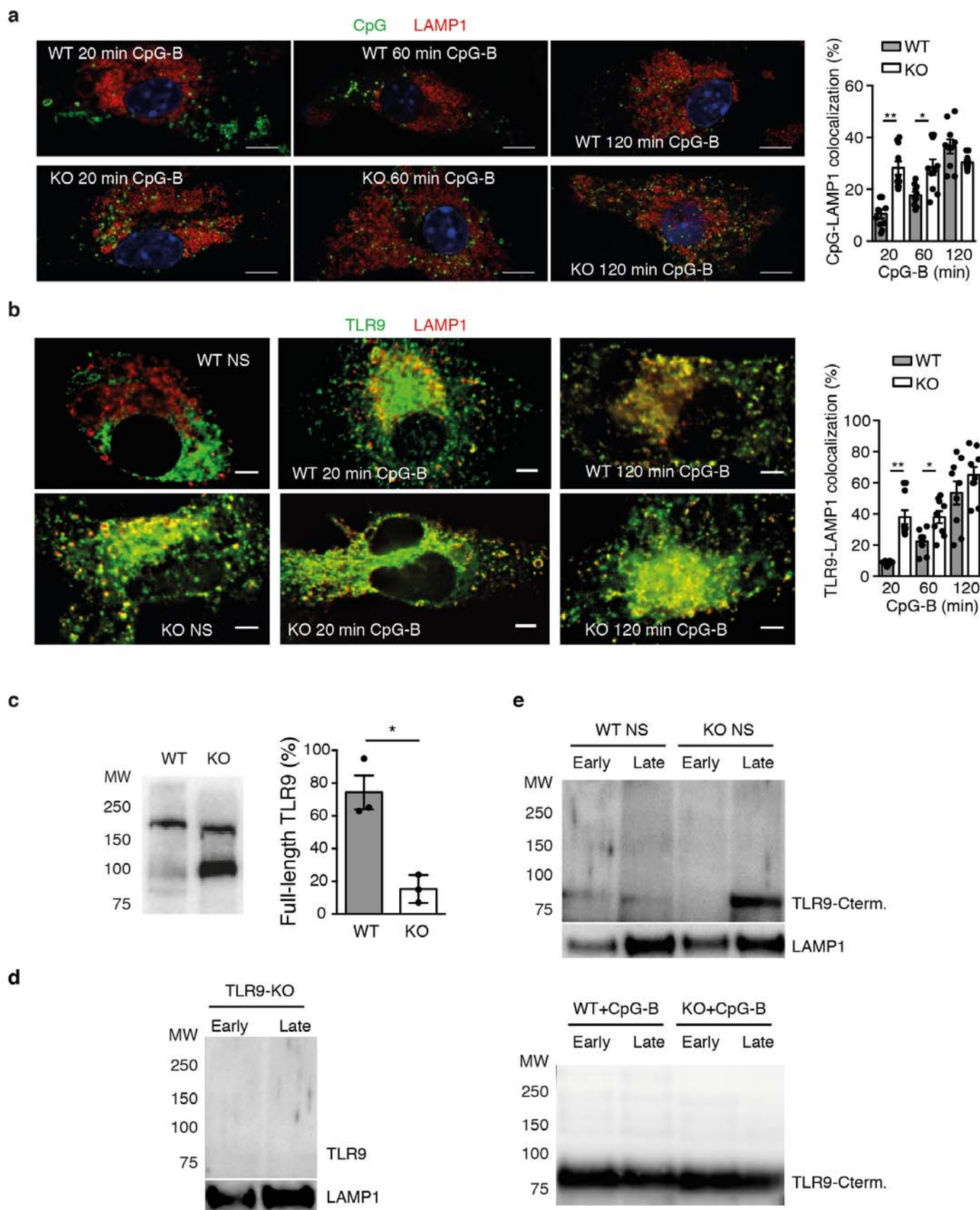


Figure 6

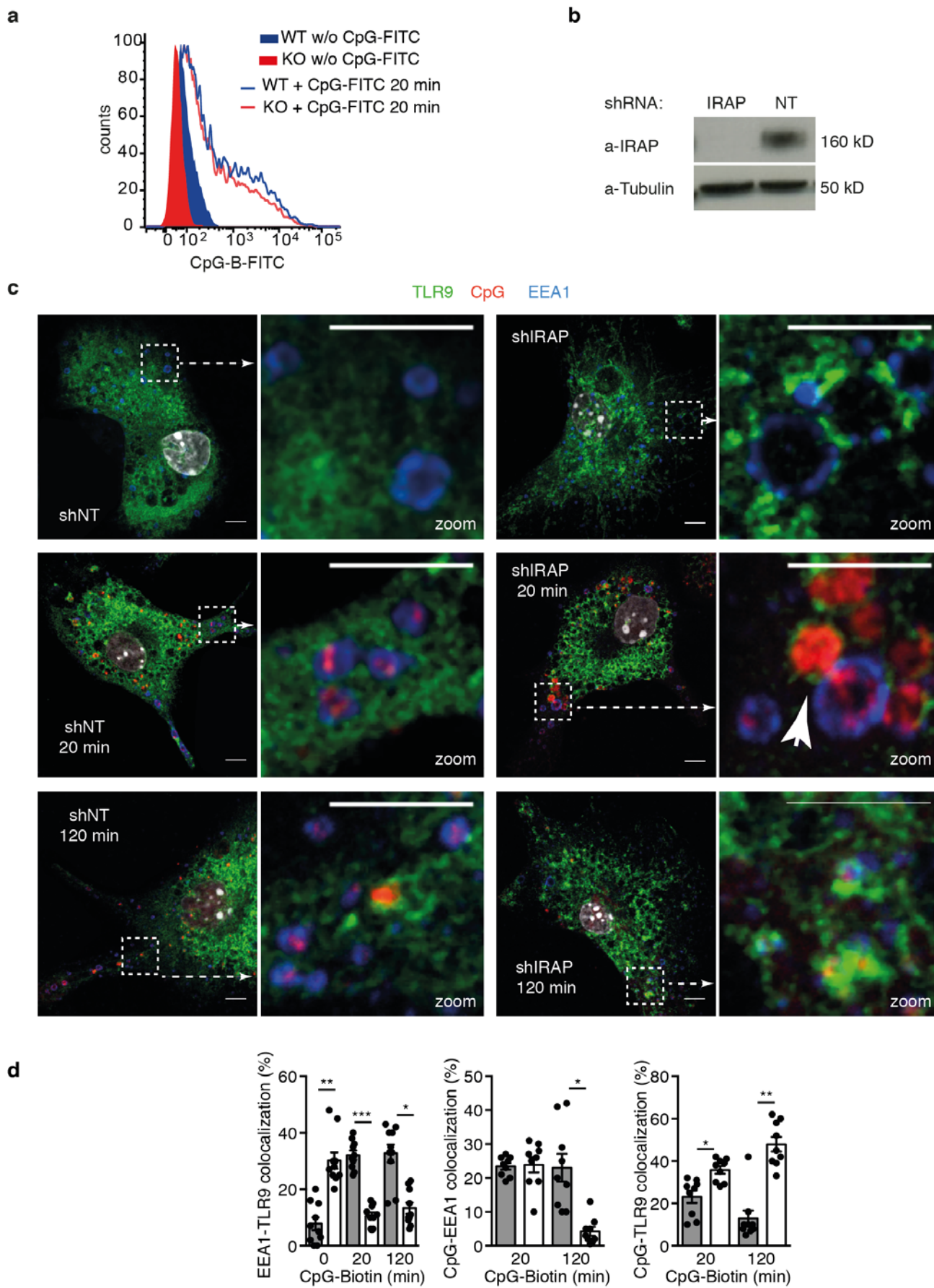


Figure 7

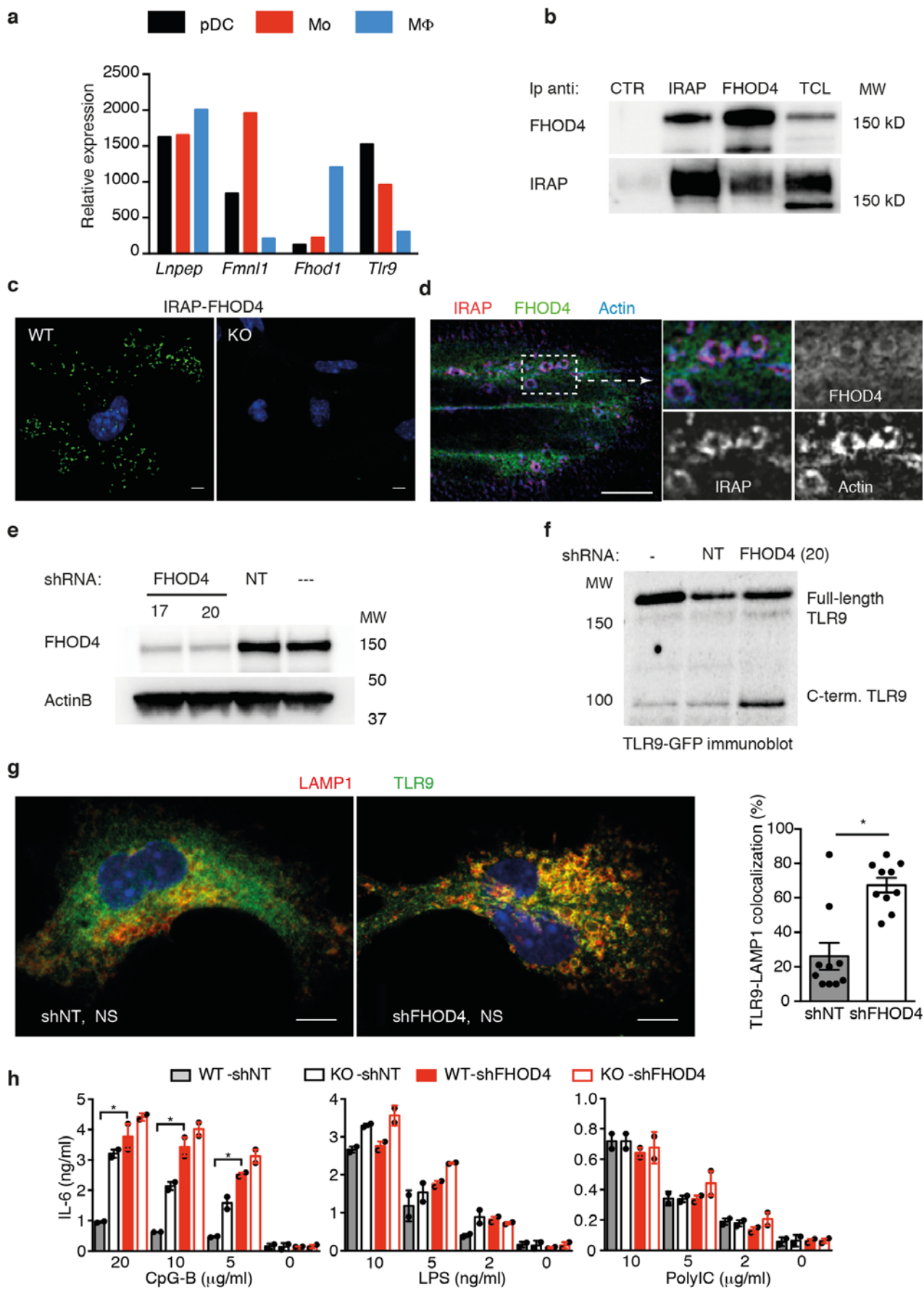


Figure 8

## **METHODS ONLINE**

### **Mice**

IRAP-deficient mice on the Sv129 background were obtained from S. Keller (Univ. of Virginia) and back-crossed 9 times to C57BL/6/J mice obtained from Janvier (St. Quentin-Fallavier, France). Mice were bred in a specific pathogen free facility and animal experiments were approved by the Comité d'éthique pour l'expérimentation animale Paris Descartes (n° P2.LS.156.10).

### **Preparation of BMDCs, MEFs, AM, spleen pDCs and cDCs**

BMDCs were generated from wild-type and IRAP-deficient mice by a 7-day culture of BM precursors in IMDM supplemented with 10% FCS, 2 mM L-glutamine, 50 mM  $\beta$ -mercaptoethanol and 20 ng/mL GM-CSF. Cell differentiation was assessed by FACS staining using anti-CD11c (N418) and CD11b (M1/70) antibodies (BD, Biosciences). MEFs were generated by trypsin dissociation of 13.5 days embryos and repetitive passages in DMEM medium containing 10% FCS, 2 mM L-glutamine, 100 U/mL penicillin and 100  $\mu$ g/mL streptomycin. The immortalized cells were used between passage 25 and 35.

Mouse AMs were isolated after lungs rinsing with PBS as described elsewhere<sup>43</sup>. The cells were plated in complete RPMI medium supplemented with 2 mM L-glutamine and 5% inactivated FCS for 24 h to allow AM adhesion<sup>44</sup>. AMs were then used for TLR stimulation assays. Mycoplasma free status of the cells was confirmed every month using the VenorGem One Step kit (Biovalley).

Spleens from wild-type and IRAP-deficient mice were digested with 500  $\mu$ g/mL Liberase DL Research grade (Roche Diagnostics, Meylan, France) and 50 ng/mL DNase I recombinant (Roche Diagnostics) in PBS. DCs were pre-enriched from splenocytes by a very-low density gradient. Briefly, splenocytes were resuspended in 5 mL of PBS containing 5 mM EDTA, 5% FCS and 18% Optiprep (Axis-Shield PoC AS) and were loaded between 5mL IMDM containing 5mM EDTA, 5% FCS and 25% Optiprep (bottom layer) and 2 mL of IMDM medium (top layer). After 20 min. of centrifugation without break at room temperature and 580 x g, the low-density fraction was collected at the interface between IMDM and 18% Optiprep. The cells were immunostained with the following antibodies: CD11b (M1/70) and GR-1 (RB6-8C5), both from BD Biosciences (Le Pont de Claix, France); CD11c (N418), CD127 (A7R34), NK1.1 (PK136), TCR Beta (H57-597), all from eBioscience (Paris, France); PDCA-1 (129-C1), CD169 (3D6.112) and F4/80 (BM8), all from BioLegend (Ozyme, Saint Quentin Yvelines, France). After exclusion of doublets, dead cells (gating on 7-Actinomycin D 7-AAD- cells) as well as B cells (CD19<sup>+</sup>), NK cells (NK1.1<sup>+</sup>) and T lymphocytes (TCR- $\beta$ <sup>+</sup>), all grouped in a “dump-channel”, pDCs (dump-, CD11b<sup>low</sup>, CD11c<sup>int</sup>, GR-1<sup>high</sup>, PDCA-1<sup>+</sup>) and cDCs (CD11b<sup>+/-</sup>CD11c<sup>high</sup>GR-1<sup>low/neg</sup>CD169<sup>neg</sup>) were sorted on a BD FACS ARIA-II with 95% purity. Alternatively, for quantitative RT-PCRs experiments, splenic pDCs were isolated with anti-mPDCA-1 magnetic beads (Miltenyi Biotech SAS Paris, France).

### **Cell stimulation and cytokine detection**

Wild-type and IRAP-deficient BMDCs, *ex-vivo* isolated splenic cDCs, pDCs and MΦs were plated in 96-well plates and treated with the indicated concentration of different compounds for 6 h or 20 h. Cytokine secretion was measured in culture supernatants with commercial (IL-6, IL-12/23(p40), TNF- $\alpha$ , eBiosciences; type I IFN, PBL Interferon Source) ELISA kits. CpG-A (CpG ODN 1585 [5'-ggG GTC AAC GTT Gag ggg gg-3']) and Imiquimod were from Invivogen (Toulouse, France), CpG-B ([5'-tga ctg tga acg ttc gag atg a-3']) was produced by TriLink Biotechnologies (Tebu-Bio, Le Perray en Yvelines, France), LPS was from Sigma-Aldrich (Lyon, France). For mRNA measurements by qRT-PCR, the cells were incubated with the different TLR ligands for 3 h. CpG-A complexes with DOTAP (Roche Diagnostics) were obtained by incubation at room temperature for 15 min.

### ***In vivo* injection with TLR ligands and *Pseudomonas Aeruginosa* (PA) infection**

Wild-type and IRAP-deficient mice were injected i.v. with 10  $\mu$ g of CpG, 1  $\mu$ g of LPS or PBS alone. Blood was collected 2 h after injection and serum was obtained by centrifugation after overnight incubation at 4°C.

*Pseudomonas aeruginosa* strain PAK (obtained from S. Lory, Harvard Medical School, Boston, MA) was prepared as previously described<sup>44</sup>. Briefly, a mid-log phase culture of PAK was centrifuged at 3.000 x g, the bacterial pellet was washed once in PBS and resuspended in PBS at the indicated concentration by measuring the OD at 600 nm. The inoculum was verified by serial dilutions plated on LB agar to determine the number of colony-forming unit (CFU). Wild-type and IRAP-deficient mice were infected intra-nasally with 1x10<sup>6</sup> CFU of PAK. Twenty-four hours after infection, the mice were sacrificed and BALs were obtained by rinsing with PBS using a blunted needle inserted into trachea. Commercial ELISA assays were used to measure IL-6, TNF (Affymetrix, eBioscience, Paris, France), CXCL1 and IL-1 $\beta$  (R&D Systems, Lille, France).

### **Quantitative RT-PCR**

Total RNA was extracted from 1 x 10<sup>6</sup> BMDCs or 0.5 x 10<sup>6</sup> pDCs with the RNeasy kit (Qiagen, Courtaboeuf, France) according to the manufacturer's instructions. One  $\mu$ g of total RNA was reverse transcribed into cDNA with the IMPROM-II Reverse Transcription System (Promega, Lyon, France) using random hexamers. Quantitative PCR was performed with

MESA FAST qPCR SYBR (Eurogentec) MasterMix using the 7900 real-time PCR instrument from Applied Biosystem.

The following primers were used to detect the pro-inflammatory cytokines and the house keeping mRNAs:

IL-6 FW : 5'-CACTCCCAACAGACCAGAGG -3'

IL-6 RV : 5'-GGTACTCCAGAAGACCAGAGG-3'

IL-12-p40 FW : 5'-GAGACTCTGAGCCACTCACA-3'

IL-12-p40 RV : 5'-GAGAGTCAGGGGAACTGCTA-3'

TNF- $\alpha$  FW : 5'-TAGCCCACGTCGTAGCAAA-3'

TNF- $\alpha$  RV : 5'-GATAGCAAATCGGCTGACGG-3'

GAPDH FW : 5'-TGGCAAAGTGGAGATTGTTGCC-3'

GAPDH RV : 5'-AAGATGGTGATGGGCTTCCCG-3'

HPRT1 FW : 5'-AGCTACTGTAATGATCAGTCAACG-3'

HPRT1 RV : 5'-AGAGGTCCTTTTCACCAGCA-3'

ACTIN-B FW : 5'-AGGTGACAGCATTGCTTCTG-3'

ACTIN-B RV : 5'-GCTGCCTCAACACCTCAAC-3'

### **Plasmid constructs and cell transfection**

TLR9-GFP plasmid was used as previously described <sup>12</sup>. Mouse UNC93B1 cDNA (Invivogen) was amplified with the following primers forward 5'-GCGGCTAGCATGGAGGTGGAGCCTC-3' and reverse 5'-GGCGCTAGCCCCTGCTCCTCAGGCC-3' (underlined NheI) and fused to N terminus of mcherry (pmCherry plasmid was a kindly gift from F. Perez, Institut Curie, Paris). The pEGFP-VAMP3 and pCDNA3.1-FHOD4 were generous gifts from F. Benvenuti and Scott Blystone, respectively. pUno-TLR3-HA plasmid was purchased from Invivogen.

For expression of fluorescent fusion proteins,  $4 \times 10^6$  MEF were electroporated with 15  $\mu$ g of plasmids in 200  $\mu$ L of PBS containing 10 mM HEPES using the GenePulser electroporator (250 kV, 900  $\mu$ F, Biorad, Marnes-la-Coquette, France). Two million BMDCs were transfected on day 6 with 1.5  $\mu$ g of plasmids coding for GFP-tagged VAMP3 or TLR9 with the AMAXA kit (Lonza, Germany). Thirty-six to 48 h after transfection, the cells were used for immunofluorescence studies or immunoblot.

### **Immunoprecipitations, Phagosome Isolation and Immunoblots**

GFP-tagged TLR9 and GFP-FHODs proteins were immunoprecipitated with GFP turbo A beads (ChromoTek, Bayern, Germany) and IRAP was immunoprecipitated with the rabbit anti-IRAP antibody kindly provided by Susanna Keller. The GFP-fusion proteins were detected on PVDF membranes with a monoclonal mouse antibody against GFP (clones 7.1 and 13.1, Roche Diagnostics). IRAP was detected on immunoblots either with the rabbit antibody provided by S. Keller, or with the mouse monoclonal antibody (3E1) from Cell Signaling Technology. Endogenous FHOD4 and FHOD1 were detected with rabbit polyclonal antibodies provided by Daniel Billadeau.

For phagosome preparation,  $10^7$  BMDCs were pulsed for 30 min at 20°C with 2.8  $\mu$ M magnetic particles (Invitrogen) and then switch to 37°C for 20 min and chased for 100 min in the presence or absence of CpG (10  $\mu$ g/ml). Cells were then washed with PBS supplemented with 0.1% BSA and mechanically disrupted by passing them through 25 g needle. Phagosomes were purified by magnetic separation, washed, and lysed. 10  $\mu$ g of proteins were submitted to separation on a 4-12% SDS NuPAGE Bis-Tris gels (Invitrogen). Proteins were transferred on a PVDF membrane and immunodetection was realized with a rabbit anti-TLR9 pAb (H-100) or a rat anti-LAMP1 from Santa Cruz and BD respectively.

### **Mutagenesis and aminopeptidase activity of IRAP**

The cDNA coding for full-length IRAP was amplified from the clone 40098425 (accession: BC120925) purchased from Dharmacon and subsequently cloned into pIRES2-EGFP (Clontech) between NheI and XhoI. The inactive form of IRAP was produced by mutagenesis with the megaprimer method<sup>45</sup> and cloned into pIRES2-EGFP. The sequence of mutagenic primer was CT AAA ATC ATT GCT CAC GCA CTG GCA CAT CAG TGG, in which the mutated base is underlined. IRAP-deficient fibroblasts were transfected by electroporation with wild-type or mutated form of IRAP, lysed in 50 mM Tris, 150mM NaCl and 1% NP-40. IRAP was immunoprecipitated with 3E1 anti-IRAP antibodies and the aminopeptidase activity on the beads was measured as previously published<sup>46</sup>.

### **Immunofluorescence microscopy**

BMDCs or MEFs were seeded on IBItreat  $\mu$ -channels (IBIDI, BioValley, Marne La Vallée, France) or fibronectin-coated slides for 6 or 16 h, respectively. For CpG internalization experiments, the cells were pulsed at 37°C with 5 mg/mL CpG-FITC or CpG-biotin (Invivogen). After the pulse, the cells were washed and incubated for additional time at 37°C.

For all experiments the cells were fixed with 4% PFA and permeabilized with 0.2% saponin in PBS containing 0.2% BSA and stained in the same buffer. Primary antibodies used were: rat anti-LAMP1 (BD Bioscience), rabbit anti-Rab14 (Sigma Aldrich), rabbit anti-Stx6 (ProteinTech), rabbit anti-IRAP (a generous gift from S. Keller, Virginia University, USA), mouse monoclonal anti-GM130 (BD Biosciences), anti-IL-12(p40) (capture antibody from ELISA Ready-set-Go! Kit) and rabbit anti-IL-6 antibody (AbDSerotec, Colmar, France). Secondary antibodies coupled with Alexa fluorochromes were from Molecular Probes (Life Technologies, Saint Aubin, France). CpG-FITC was visualized with goat anti-FITC antibodies (Molecular Probes) and CpG-Biotin was visualized with Alexa594-streptavidin (Molecular Probes). Images were acquired on a Leica SP8 confocal microscope or, where specified, on a Leica DMI 6000 microscope equipped with a piezoelectric-driven stage and Optophotonics XF100-2 (FITC), XF102-2 (Texas Red) and XF06 (DAPI) filters. Image treatment and analysis were performed with Image J software.

### **Proximity ligation assay (Duolink)**

Duolink™ (OLINK Bioscience) was performed according to the manufacturer's instructions. Briefly, the cells were grown on fibronectin-coated coverslips, fixed for 10 min in 2% paraformaldehyde at 37°C, permeabilized in PBS, 0.05% saponin, 0.2% BSA for 10 min and blocked with 3% BSA in PBS. Primary antibodies used were mouse anti-GFP (Roche Diagnostics, mix of clones 7.1 and 13.1), rabbit anti-IRAP, rabbit anti-FHOD4 (a gift from D. Billadeau), mouse anti-IRAP clone 3E1 (Cell Signaling Technology), mouse anti-MyD88 (Abcam), rabbit anti-NF- $\kappa$ B (RelA C20 from Santa Cruz) and rabbit anti-IRF7 (EPR 4718 Abcam). After washing the cells, PLA probes were added, followed by hybridization, ligation, and amplification for 90 min at 37°C. Nuclear DNA (DAPI labeling) and protein interactions were visualized after incubation with the detection solution. Fluorescence signal was acquired on a Leica SP8 confocal microscope.

### **Detection of ERK1/2 and I- $\kappa$ B- $\alpha$ phosphorylation**

BMDCs were incubated for different times with CpG (10  $\mu$ g/ml) or LPS (100 ng/ml) and lysed in RIPA buffer containing a complete proteases and phosphatase inhibitor cocktail (Roche). Proteins were quantified by with Pierce BCA Protein assay (Thermo scientific). 25  $\mu$ g of proteins were loaded on a 4-12% SDS NuPAGE Bis-Tris gels (Invitrogen) and transferred on a PVDF membrane. Immunodetection was realized with rabbit anti-p44/42

MAPK (ERK1/2, 137F5), mouse anti phospho-p44/42 MAPK (p-ERK1/2, E10) (Thr202/Tyr204) from Cell Signaling Technology. Total I- $\kappa$ B- $\alpha$  and phospho I- $\kappa$ B- $\alpha$  were measured with a Pathscan Sandwich ELISA kit (Cell Signaling Technology).

### **Lentiviral shRNA knock-down of FHOD4 and IRAP**

The pLK0.1-puromycin plasmids coding for *Lnpep* specific shRNA (TRCN0000031113), *Fmnl1* specific shRNA (TRCN0000120520 and TRCN0000120517), *Fhod1* specific shRNA (TRCN0000257842, TRCN0000216791, TRCN0000248947, TRCN0000248949, TRCN0000192602) and a non-targeting shRNA (shNT) were purchased from Sigma Aldrich. The lentiviral particles were produced according to the protocol published by Tiscornia G. *et al*<sup>47</sup>. BM precursor cells were seeded in 96 wells plate at 10<sup>5</sup> cells per well. They were transduced on the second day of differentiation using the MOI of 10, in the presence of 8  $\mu$ g/mL polybrene. Following 2 h centrifugation at 37°C and 950xg, the lentiviral mix was replaced with BMDCs differentiation medium. On day 5 of differentiation, the non-transduced cells were eliminated by puromycin (5 $\mu$ g/mL) selection for 48 h. The cells were analyzed between day 7 and 9 of differentiation.

### **Statistical analysis**

Statistical analysis was performed using Prism software (Graph Pad software). Unpaired, two-tailed Student's t tests were used for comparison of two groups. P values<0.05 were considered significant. Mantel-Cox test was used for comparison of mice survival.

### **Data availability**

The data that support the findings of this report are available from the corresponding authors upon request.

### **References:**

- 43 Goncalves de Moraes, V. L., Singer, M., Vargaftig, B. B. & Chignard, M. Effects of rolipram on cyclic AMP levels in alveolar macrophages and lipopolysaccharide-induced inflammation in mouse lung. *Br J Pharmacol* **123**, 631-636, doi:10.1038/sj.bjp.0701649 (1998).
- 44 Descamps, D. *et al.* Toll-like receptor 5 (TLR5), IL-1beta secretion, and asparagine endopeptidase are critical factors for alveolar macrophage phagocytosis and bacterial killing. *Proc Natl Acad Sci U S A* **109**, 1619-1624, doi:10.1073/pnas.1108464109 (2012).

- 45 Vander Kooi, C. W. Megaprimer method for mutagenesis of DNA. *Methods Enzymol* **529**, 259-269, doi:10.1016/b978-0-12-418687-3.00021-5 (2013).
- 46 Saveanu, L. *et al.* Concerted peptide trimming by human ERAP1 and ERAP2 aminopeptidase complexes in the endoplasmic reticulum. *Nat Immunol* **6**, 689-697, doi:10.1038/ni1208 (2005).
- 47 Tiscornia, G., Singer, O. & Verma, I. M. Production and purification of lentiviral vectors. *Nat Protoc* **1**, 241-245, doi:10.1038/nprot.2006.37 (2006).